RSC Advances

PAPER

View Article Online
View Journal | View Issue

Cite this: *RSC Adv.*, 2025, **15**, 19369

Highly sensitive spider-slit-organ-inspired crack-based flexible temperature sensor†

Ping Li, *[ab] Yi Yang,[b] Jing Chen,[b] Libo Zhao*[c] and Tianling Ren*[b]

Received 7th April 2025
Accepted 20th May 2025

DOI: 10.1039/d5ra02392k

rsc.li/rsc-advances

We found that a spider-slit-inspired bionic structure is not only sensitive to tiny vibrations but also exhibits remarkable sensitivity to temperature changes, as confirmed through testing. Based on these findings, we propose a bionic, crack-based graphene temperature sensor, whose temperature sensitivity reaches 9.93 × 10^{-3} °C^{-1}. We studied the influence of the thickness of the PDMS substrate and the laser-scribing angle on the performance of the sensor; the optimized parameter for the thickness of the PDMS substrate is 400 μm, and the laser-scribing angle is $\theta = 0$. Meanwhile, the proposed graphene-based temperature sensor has great clinical potential for the real-time monitoring of human body temperature, and it also can be used for water/liquid temperature-change measurements and food-storage temperature detection.

Introduction

The recent spread of epidemics has renewed interest in flexible temperature sensors within the medical field, due to their wearability and the ability to monitor local temperature changes in real time regardless of large-scale motion by the human body. Recently, flexible temperature sensors are usually fabricated using metals, such as Pt, Ag, and Ni as sensitive components,[1–5] which are expensive, environmentally polluting, and biologically unfriendly. Nanomaterial-based flexible temperature sensors can effectively improve these shortcomings in terms of economy and biocompatibility. In 2015, Yokota *et al.* proposed ultraflexible and printable temperature sensors based on composites of semicrystalline acrylate polymers and graphite with a high sensitivity of 20 mK, which exhibit a high temperature coefficient of resistance and repeatability (1800 times) between 25 °C and 50 °C.[6] In 2013, Rogers *et al.* introduced ultrathin, compliant skin-like arrays of precise temperature sensors and heaters, which can provide continuous, non-invasive spatial mapping of skin temperature with millikelvin precision, and they allow the simultaneous quantitative assessment of tissue thermal conductivity. Together with other measurements, these devices provide meaningful information for the clinical diagnosis of related diseases, like cardiovascular health, malignancy and so on.[7]

Cupiennius salei is a large Central American wandering spider that lives on plants such as bromeliads, and it has lyriform slit organs located near the leg joint to detect vibrations in its surroundings.[8–10] The unique lyriform geometry of the slit organs can respond to tiny changes in external forces, resulting in ultrasensitive displacement detection and good mechanical compliance. Inspired by the slit organs of the spider, Kang *et al.* developed an ultrasensitive mechanical sensor based on nanoscale crack junctions, which has a gauge factor of more than 2000 in the 0–2% strain range and a minimum vibration amplitude of 10 nm, and it can detect human physiological signals, such as voice patterns and heart rate and small changes in external forces.[11]

During testing, we found that the spider-inspired crack-based bionic structure mentioned above not only works for vibration detection but is also sensitive to temperature changes. Therefore, we proposed a spider-slit-inspired crack-based graphene temperature sensor (SCGTS) here, which is mainly composed of PDMS thin film and graphene film with a microcrack structure. The working principle is that during a temperature change, thermal stress is generated due to the difference in expansion coefficients of the different materials, and the resulting stress can be characterized by resistance changes of the crack-based graphene film.

Results and discussion

A schematic diagram of the working principle of the crack-based flexible temperature sensor is shown in Fig. 1; the sensor is mainly formed from PDMS film as the substrate with graphene film with a continuous microcrack structure as the conductive layer. The graphene film is fabricated by a laser scribing process.[12,13] As shown in Fig. 1b, the working principle of the sensor is that, during a temperature increase in the

[a]*School of Intelligent Manufacturing and Smart Transportation, Wenzheng College of Suzhou University, Suzhou, 215104, China. E-mail: lpxiaomi@szcu.edu.cn*

[b]*Institute of Microelectronics and Beijing National Research Center for Information Science and Technology (BNRist), Tsinghua University, Beijing 100084, China. E-mail: Rentl@tsinghua.edu.cn*

[c]*School of Mechanical Engineering, Xi'an Jiaotong University, Xi'an 710049, China. E-mail: libozhao@mail.xjtu.edu.cn*

† Electronic supplementary information (ESI) available. See DOI: https://doi.org/10.1039/d5ra02392k

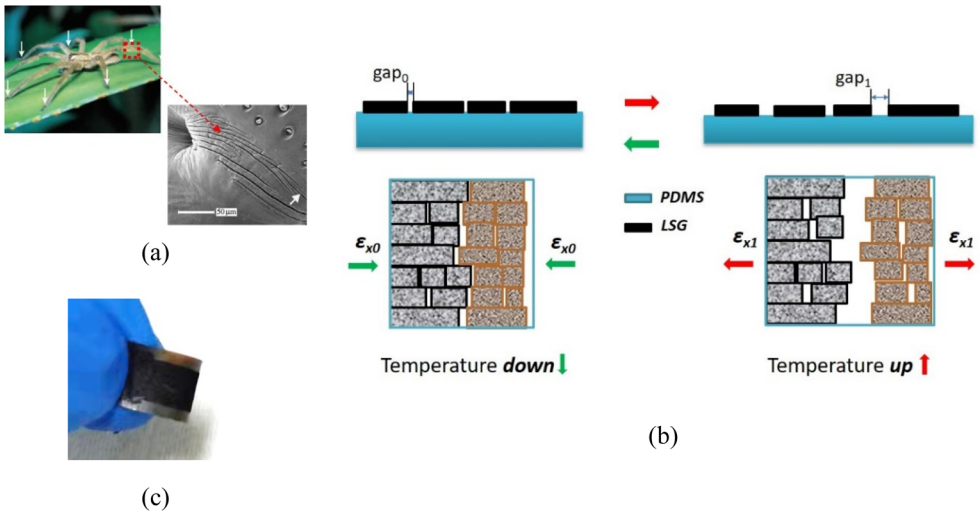

Fig. 1 Schematic diagrams of the principle of the crack-based graphene temperature sensor. (a) A schematic diagram of the structure of the spider lyriform organs. (b) The working principle of the crack-based flexible sensor when the ambient temperature goes up and down. (c) A picture of the fabricated graphene sensor.

surroundings, the PDMS and graphene films undergo thermal expansion and thermal stress ε_{x_1} is generated due to differences in the expansion coefficients of the two materials. The graphene film here has a structure with a series of tiny, parallel, spider-slit-like microcracks; when stress ε_{x_1} is generated, the graphene crack gaps increase from an initial value of gap_0 to gap_1, and the macro-resistance of the crack-based graphene film decreases with the increase in crack gaps. A similar but reverse process occurs for a temperature decrease.

The fabricated graphene sensor is shown in Fig. 1c and a schematic illustration of the fabrication process is demonstrated in Fig. 2a. First, graphene oxide (GO) aqueous solution (2 mg mL^{-1}, 1–5 layers) diluted with 16.67% (volume ratio) tetrahydrofuran was drop-coated onto the PDMS substrate, forming GO film after vaporization in a fume hood for approximately 48 h. Then, the GO/PDMS film was placed under a commercial laser-patterning device; the laser transforms GO to laser-scribed graphene (LSG), which is a kind of multilayer reduced graphene oxide (rGO) working as the sensing component of the SCGTS. The LSG/PDMS film was then roll-stretched on a 1 mm-diameter metal rod by applying a tensile force at a speed of 2 mm s^{-1}, and the spider-cracks formed and expanded along the film in the longitudinal direction in this process. Finally, after adding electrical connections using silver paste and copper wires, the temperature sensor was obtained.

Fig. 2b and c show scanning electron microscope (SEM) images of the graphene film before and after laser scribing, respectively. It can be clearly seen that the GO film is transformed to multilayer rGO nanosheets, which stacked as continuous island-like structures. In addition, after being roll-stretched on the metal rod, the spider-slit-like parallel microcrack structure is generated, and the gaps between rGO nanosheets are magnified, as shown in Fig. S1.† The Raman spectrum of LSG is shown in Fig. 2d. Due to the laser transformation process, the reduction rate of GO is not very high, and the intensity of the 2D peak in the LSG Raman spectrum is lower, while the intensities of the D peak and G peak, which are related to GO, are larger compared with the typical Raman spectrum of monolayer graphene.[14]

To investigate the temperature–resistance characteristics of SCGTS, a set of sensor samples was fabricated with a rectangular graphene sensing pattern of 2 mm × 0.6 mm. In tests, the microcrack structure of the graphene film worked as a mechanical amplifier, which made SCGTS show high sensitivity and good linearity. As shown in Fig. 1b, SCGTS works like a thermistor temperature sensor, and the temperature coefficient of resistance (TCR), which is generally used to characterize the sensitivity of a thermistor, is expressed as follows:

$$\mathrm{TCR} = \mathrm{d}R/R \times \mathrm{d}T = (R_\mathrm{f} - R_0)/R_0 \times (T_\mathrm{f} - T_0)$$

where $\mathrm{d}R$ represents the change in resistance and $\mathrm{d}T$ represents the change in temperature, R_0 is the resistance of the sensor at the initial temperature T_0, and R_f is the resistance of the sensor when the temperature rises to T_f.

The temperature–resistance characteristics of the sensor were mainly tested by the platform shown in Fig. 3a, which was mainly composed of a data acquisition unit, a temperature control bench (the accuracy reaches 0.01 $°C^{-1}$) and Fluke 1586A apparatus to monitor the change in resistance. The experimental temperature was changed every 5 min at 5 °C intervals in the range of 22–100 °C, and the change in sensor resistance was recorded in the meantime. The temperature sensitivity values of several samples, S_1, S_2, and S_3 (the thickness of the PDMS substrate is 400 μm), were obtained, and the results are shown in Fig. 3b. Due to differences in the microcracks formed in the graphene film of each sample, the sensor performance varied, and the measured temperature sensitivities S_1, S_2, and S_3 are 2.02×10^{-3}, 9.09×10^{-3}, and 9.93×10^{-3} $°C^{-1}$, respectively. The corresponding linear correlation coefficients (adj. R-square)

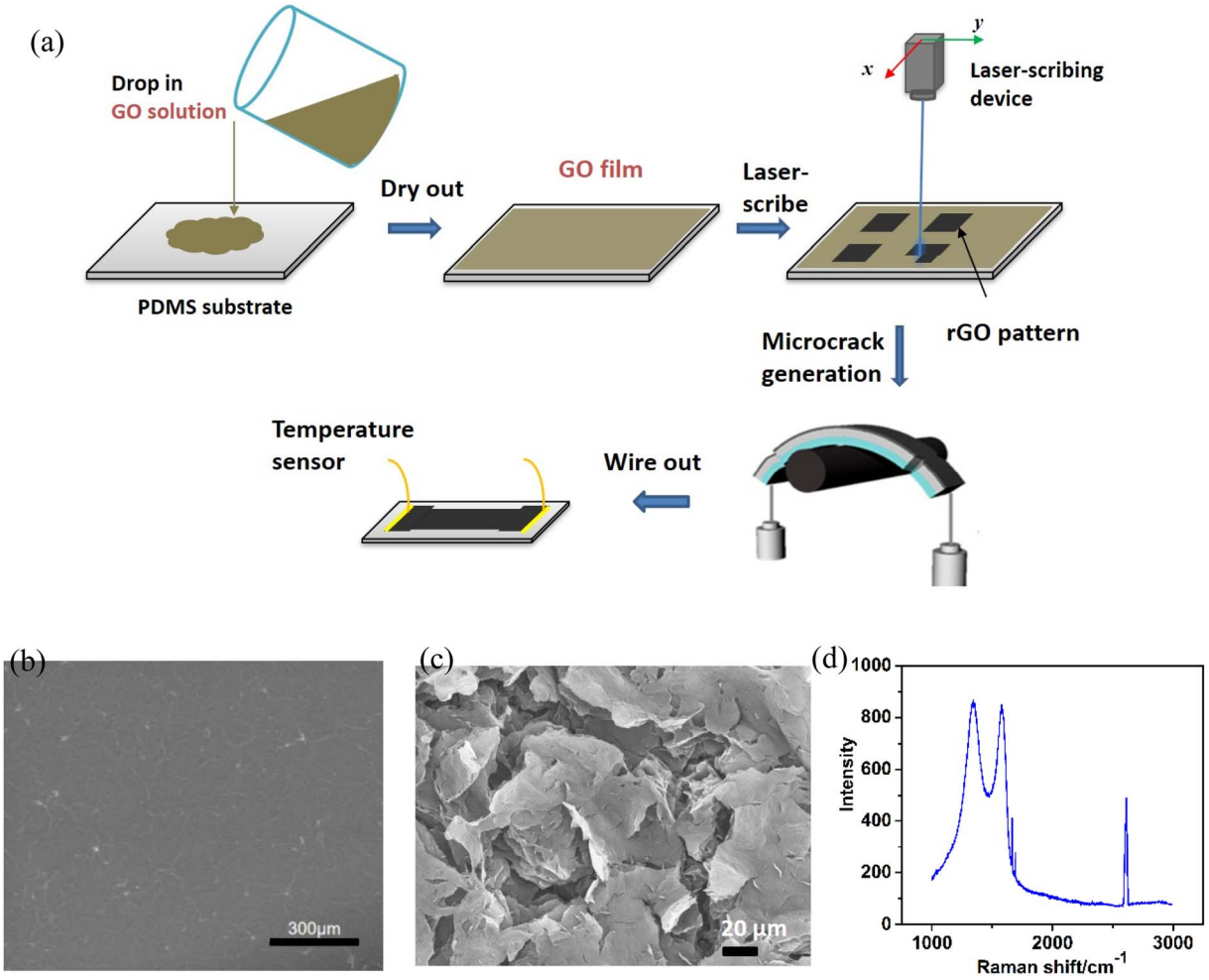

Fig. 2 The manufacturing process and structure of SCGTS. (a) A schematic diagram of the process for the efficient and low-cost fabrication[13] of SCGTS and the generation of microcracks in the graphene film. (b) and (c) SEM images of GO and laser-scribed rGO. (d) The Raman spectrum of LSG.

were 0.9882, 0.99431, and 0.9648, in the range of 25 °C to 100 °C. The graphene flexible temperature sensor prepared in this paper has ultrahigh sensitivity compared to a metal-film-based flexible sensor (TCR = 2.78×10^{-3} °C^{-1}), and the TCR can reach up to 9.93×10^{-3} °C^{-1}.

Due to the obvious improvement in conductivity when Ag nanowires doped into the graphene film, here Ag nanowires (10 mg mL^{-1} with an average length of 20 mm and an average diameter of 90 nm, volume ratio 1 : 10) were doped into the graphene to achieve further performance improvements in the proposed SCGTS. The testing results are shown in Fig. 3c; the graphene flexible sensor doped with Ag nanowires exhibits a negative resistance-temperature response, and the temperature sensitivity decreases only to $S_{Ag} = -1.95 \times 10^{-3}$ °C^{-1} with linearity of 0.9991. It can be seen that Ag nanowire doping does not improve the performance of the temperature sensor, but it reduces the temperature sensitivity, which may be caused by an oxidation effect from the Ag nanowires as the temperature increases.

The effect of the thickness of the PDMS substrate on the performance of SCGTS was investigated, and the test results are shown in Fig. 3d. We can see that, in the case of different thicknesses of PDMS, as the thickness gradually increases from 200 μm to 400 μm, the measured temperature sensitivity of SCGTS also increases from 0.96×10^{-3} °C^{-1} to 2.06×10^{-3} °C^{-1} to 4.34×10^{-3} °C^{-1}, respectively. From the results above, it can be seen that SCGTS has higher temperature sensitivity when the thickness of PDMS is 400 μm and a PDMS substrate with a thickness of 400 μm is used in all following application experiments.

In the laser scribing process, we found that changing the laser-scribing angle θ as defined in Fig. 3f can influence the resistance performance of the graphene sensor. The reason is that the programmable laser-scribing machine utilizes two stepper motors to control the movement of the laser beam in two directions, X and Y. The laser can only scribe in rows one-by-one in one direction each time, and the LSG obtained is composed of stacked parallel graphene ribbons along one direction, like X or Y. In this paper, we changed the scribing

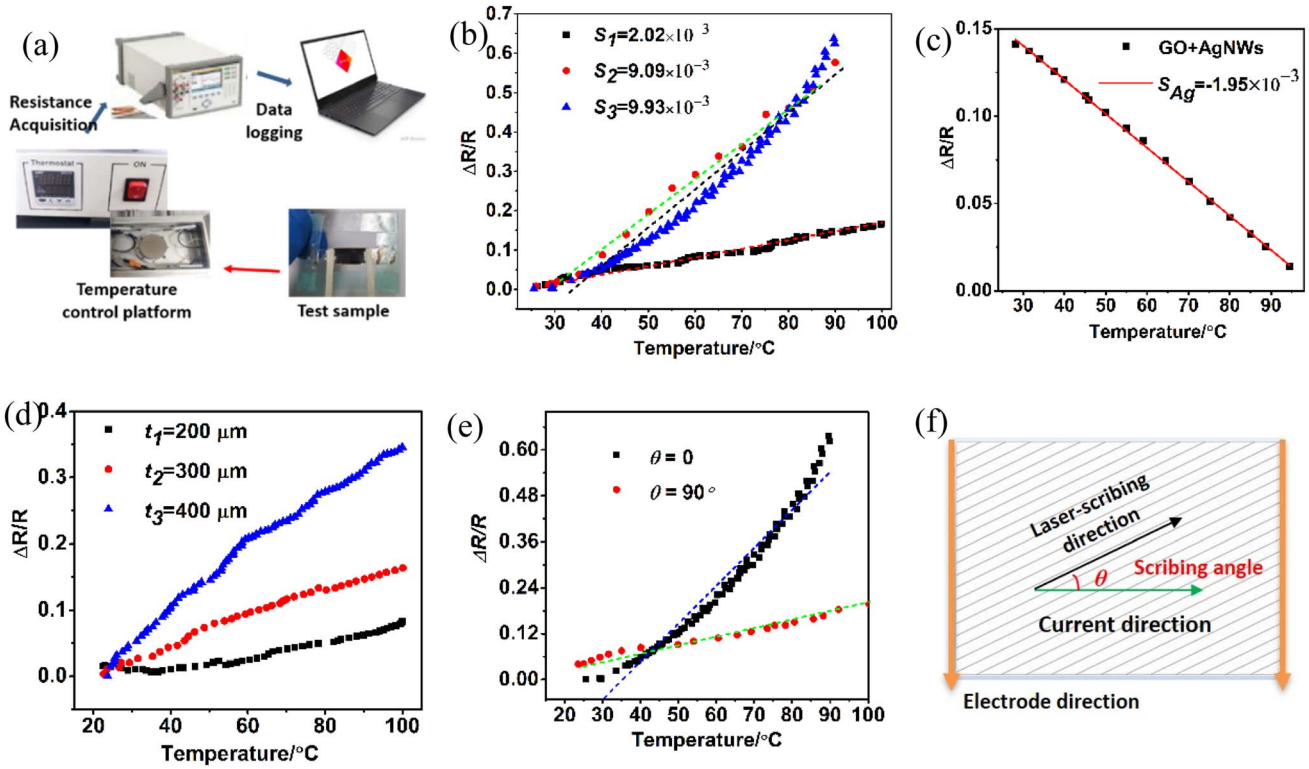

Fig. 3 The temperature–resistance characteristic testing of the flexible sensors. (a) A schematic diagram of the testing platform. (b) Temperature sensitivity results for three different samples. (c) Sensitivity testing of a graphene temperature sensor doped with Ag nanowires. (d) Results for graphene temperature sensors with different PDMS substrate thicknesses. (e) Sensitivity results as the laser angle changed from 0 to 90° and (f) a schematic illustration of the scribing angle.

angle to 90°and tested the performance of the prepared graphene temperature sensor. As shown in Fig. 3e, when θ is changed from 0 to 90°, the temperature sensitivity decreases from 9.90×10^{-3} °C^{-1} to $S_{90} = 1.89 \times 10^{-3}$ °C^{-1}. This is mainly because a change in the laser-scribing angle leads to a structure change of the laser-reduced LSG film, and the resistance of the LSG increased, leading to a significant decrease in temperature sensitivity.

Applications

Taking the flexible sensor inspired by spider bionic structures proposed in this article, we explored relevant applications, including the real-time detection of human body temperature, monitoring the hot water cooling process, and food preservation temperature detection under different conditions. The SCGTS prepared is based on LSG/PDMS film, which shows good flexibility and stretchability, and it can be conformally attached to the surface of human skin, as shown in Fig. 4(a). The temperature sensor was attached to the back of a female (30 years old, basal body temperature: 36.4 °C) subject's hand, and the resistance changes of the sensor were recorded and temperature changes on the upper surface of the sensor film were simultaneously detected using an infrared thermometer. The test results from the clinically used infrared thermometer and from SCGTS show good agreement, indicating that applying SCGTS to continuously measure the body surface temperature is reliable and feasible.

SCGTS was pasted on the outer surface of a container that was used to monitor the temperature changes during the natural cooling process of hot coffee and the accelerated cooling process of hot water after ice was added. Meanwhile, an electronic food thermometer was used to measure the real-time temperatures of the liquids to serve as a reference. As shown in Fig. 4b, 50 ccs of hot coffee gradually cools from 76 °C to about 38 °C in 50 min, and the cooling rate is faster at temperatures above 50 °C, which is ~1.3°C min^{-1}. The resistance of SCGTS attached to the outer wall of the plastic bottle also decreases with temperature showing the same trend, from 5 kΩ to 2.5 kΩ, and the rate of decline above 50 °C is also faster. The hot coffee gradually cooled from 50 °C to ~38 °C within 20–50 min, with a slow cooling rate of 0.43 °C min^{-1}. The resistance value of the SCGTS also decreases more slowly, from 2.5 kΩ to ~1.25 kΩ.

As shown in Fig. 4c, about 150 mL of hot water was added to a beaker, and the prepared SCGTS was pasted on the outer wall of the beaker; the resistance change of the graphene sensor was detected while simultaneously measuring the temperature changes in water. The hot water in the beaker gradually cooled from 76 °C to 22 °C from 0–43 min, and the resistance value of the graphene temperature sensor on the outer wall also decreased from 1.4 kΩ to 0.75 kΩ; the trend of decrease of the

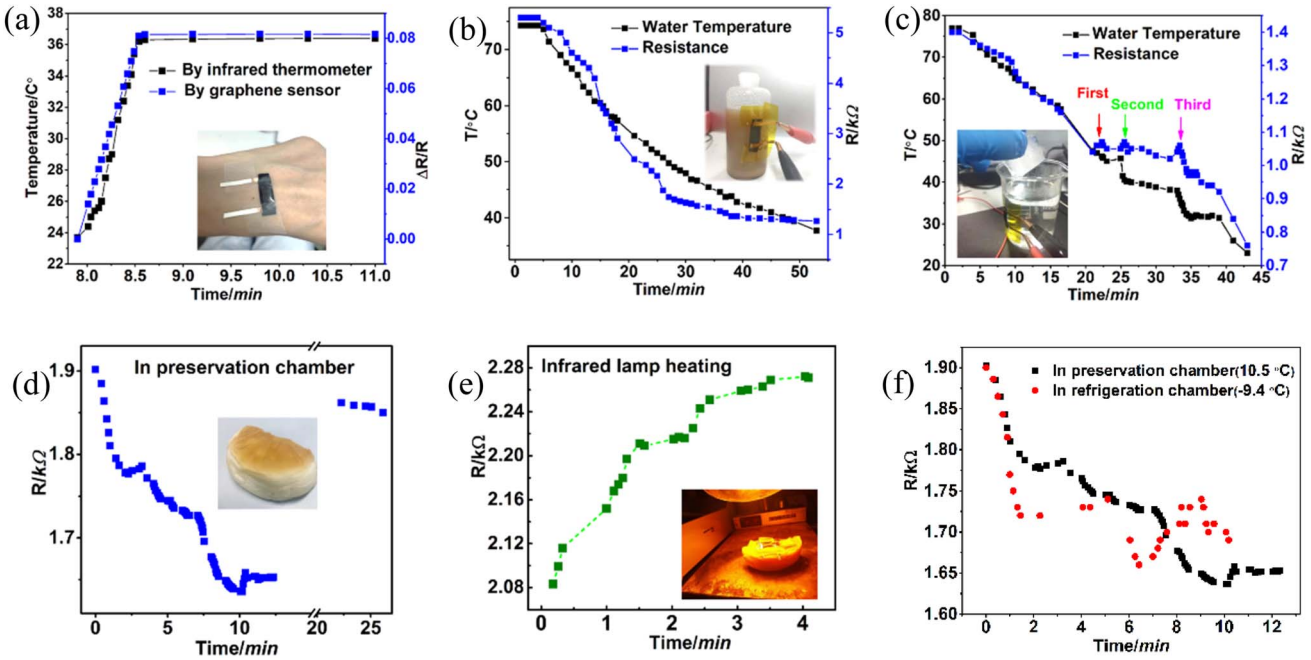

Fig. 4 (a) The real-time detection of human body surface temperature. (b) The real-time temperature detection of the cooling process of hot coffee. (c) The real-time temperature detection of the cooling process after adding ice to hot water. (d) The temperature-change process of bread kept in a refrigerator's fresh-keeping compartment. (e) The temperature change of the surface of bread which was heated by an infrared lamp. (f) The temperature-change process for bread that was kept in the refrigerator's fresh-keeping compartment and in the freezer chamber, respectively.

resistance is very close to the trend of decrease for the water temperature. During the measurements, ice cubes were added to the hot water three times to accelerate the cooling process. It can be clearly observed in the right part of Fig. 4c that each time an ice cube is added into the hot water, an aggressive heat exchange phenomenon is triggered, causing an obvious fluctuation in water temperature. This fluctuation can be clearly observed from the blue curve. The experimental results above show that the prepared SCGTS can be used for the real-time monitoring of water-temperature changes; if integrated with water cups or feeding bottles, it can achieve real-time water-temperature detection and help avoid scalding when drinking hot water or feeding infants.

In the process of food preservation and transportation, the storage temperature is very critical, and improper temperature control can easily cause food deterioration and spoilage. Here, the prepared SCGTS was pasted on the surface of a piece of bread to test the food storage temperature under different storage conditions. As can be seen from Fig. 4d, when the bread is put into the fresh-keeping compartment of a refrigerator (the internal temperature is measured to be ~10.5 °C), due to the large temperature difference between the fresh-keeping compartment and the external environment (the room temperature is ~22 °C), the measured temperature decreases rapidly; the resistance of the graphene temperature sensor also decreases and drops to its lowest value after 10 min. After another 5 min, the bread was taken out and placed in the environment, and the resistance value of the graphene sensor returned to its initial state rapidly. From the comparison shown in Fig. 4f, when the bread was put into the freezer chamber of the refrigerator, due to the lower temperature (only −9.4 °C), the resistance of the graphene temperature sensor decreased faster than that of bread in the fresh-keeping compartment, especially for the drop to the lowest value within 0–2 min. As shown in Fig. 4e, when the bread is heated under an infrared lamp, the resistance of the graphene temperature sensor increases with the increase in temperature, and the resistance gradually tends to stabilize when the set temperature (~70 °C) is reached within 3–4 min. These results show that the graphene flexible sensor prepared can reliably and stably achieve the real-time detection of food storage temperatures.

Conclusions

In this paper, we propose a graphene flexible temperature sensor based on a spider-crack bionic structure. We conducted sensor performance tests and application experiments and studied the influence of PDMS substrate thickness and laser-scribing angle on the performance of the sensor. The temperature sensor has high sensitivity, which can reach up to 9.93 × 10^{-3} °C^{-1}. The optimized parameters for the temperature sensor are a PDMS substrate thickness of 400 μm and a laser-scribing angle θ of 0°. The prepared graphene temperature sensor has great potential for application in real-time temperature measurements, like water/liquid temperature-change measurements and food-storage temperature detection; also, it can be applied clinically for the real-time monitoring of human body temperature.

Data availability

The authors confirm that the data supporting the findings of this study are available within the article and its ESI.†

Conflicts of interest

There are no conflicts to declare.

Acknowledgements

This work was supported by the National Key R&D Program (2021YFC3002200, 2020YFA0709800, 2018YFC2001202), and the National Natural Science Foundation of China (U20A20168,61874065, 51861145202). The authors are also thankful for the support of the Tsinghua University Initiative Scientific Research Program, the Beijing Innovation Center for Future Chip, Beijing Natural Science Foundation (4184091).

References

1 L. Gwo-Bin, H. Fu-Chun, L. Chia-Yen and M. Jiun-Jih, *Acta Mech. Sin.*, 2004, **20**, 140–145.
2 T. Someya, Y. Kato, T. Sekitani, S. Iba, Y. Noguchi, Y. Murase, H. Kawaguchi and T. Sakurai, *Proc. Natl. Acad. Sci. U. S. A.*, 2005, **102**, 12321–12325.
3 M. D. Dankoco, G. Y. Tesfay, E. Benevent and M. Bendahan, *Mater. Sci. Eng. B*, 2016, **205**, 1–5.
4 Y. Su, C. Ma, J. Chen, H. Wu, W. Luo, Y. Peng, Z. Luo, L. Li, Y. Tan, O. M. Omisore, Z. Zhu, L. Wang and H. Li, *Nanoscale Res. Lett.*, 2020, **15**, 200.
5 Y. Chen, B. Lu, Y. Chen and X. Feng, *Sci. Rep.*, 2015, **5**, 11505.
6 T. Yokota, Y. Inoue, Y. Terakawa, J. Reeder, M. Kaltenbrunner, T. Ware, K. Yang, K. Mabuchi, T. Murakawa, M. Sekino, W. Voit, T. Sekitani and T. Someya, *Proc. Natl. Acad. Sci. U. S. A.*, 2015, **112**, 14533–14538.
7 R. C. Webb, A. P. Bonifas, A. Behnaz, Y. Zhang, K. J. Yu, H. Cheng, M. Shi, Z. Bian, Z. Liu, Y.-S. Kim, W.-H. Yeo, J. S. Park, J. Song, Y. Li, Y. Huang, A. M. Gorbach and J. A. Rogers, *Nat. Mater.*, 2013, **12**, 938–944.
8 P. Fratzl and F. G. Barth, *Nature*, 2009, **462**, 442–448.
9 B. Hößl, H. J. Böhm, F. G. Rammerstorfer, R. Müllan and F. G. Barth, *J. Biomech.*, 2006, **39**, 1761–1768.
10 B. Park, J. Kim, D. Kang, C. Jeong, K. S. Kim, J. U. Kim, P. J. Yoo and T.-i. Kim, *Adv. Mater.*, 2016, **28**, 8068.
11 D. Kang, P. V. Pikhitsa, Y. W. Choi, C. Lee, S. S. Shin, L. Piao, B. Park, K.-Y. Suh, T.-i. Kim and M. Choi, *Nature*, 2014, **516**, 222–226.
12 Q. Wu, Y. Qiao, R. Guo, S. Naveed, T. Hirtz, X. Li, Y. Fu, Y. Wei, G. Deng, Y. Yang, X. Wu and T.-l. Ren, *ACS Nano*, 2020, 6.
13 Y. Qiao, X. Li, J. Jian, Q. Wu, Y. Wei, H. Shuai, T. Hirtz, Y. Zhi, G. Deng, Y. Wang, G. Gou, J. Xu, T. Cui, H. Tian, Y. Yang and T.-L. Ren, *ACS Appl. Mater. Interfaces*, 2020, **12**, 49945–49956.
14 L. M. Malard, M. A. Pimenta, G. Dresselhaus and M. S. Dresselhaus, *Phys. Rep.*, 2009, **473**, 51–87.